Nano Energy (2015) 17, 196–205

Available online at www.sciencedirect.com

ScienceDirect

journal homepage: www.elsevier.com/locate/nanoenergy

COMMUNICATION

Hybrid tandem solar cells with depleted-heterojunction quantum dot and polymer bulk heterojunction subcells

Taesoo Kim[a], Yangqin Gao[a], Hanlin Hu[a], Buyi Yan[a], Zhijun Ning[b,c], Lethy Krishnan Jagadamma[a], Kui Zhao[a], Ahmad R. Kirmani[a], Jessica Eid[a], Michael M. Adachi[b], Edward H. Sargent[b], Pierre M. Beaujuge[a,*], Aram Amassian[a,*]

[a]*Physical Sciences and Engineering Division, Solar and Photovoltaics Engineering Research Center (SPERC), King Abdullah University of Science and Technology (KAUST), Thuwal 23955-6900, Saudi Arabia*
[b]*Department of Electrical and Computer Engineering, University of Toronto, 10 King's College Road, Toronto, ON, Canada M5S 3G4*
[c]*School of Physical Science and Technology, ShanghaiTech University, 100 Haike Road, Shanghai 201210, China*

Received 1 June 2015; received in revised form 30 July 2015; accepted 21 August 2015
Available online 1 September 2015

KEYWORDS
Hybrid tandem solar cells;
Colloidal quantum dot;
Polymer;
Conjugated polyelectrolyte

Abstract
We investigate hybrid tandem solar cells that rely on the combination of solution-processed depleted-heterojunction colloidal quantum dot (CQD) and bulk heterojunction polymer:fullerene subcells. The hybrid tandem solar cell is monolithically integrated and electrically connected in series with a suitable p-n recombination layer that includes metal oxides and a conjugated polyelectrolyte. We discuss the monolithic integration of the subcells, taking into account solvent interactions with underlayers and associated constraints on the tandem architecture, and show that an adequate device configuration consists of a low bandgap CQD bottom cell and a high bandgap polymer:fullerene top cell. Once we optimize the recombination layer and individual subcells, the hybrid tandem device reaches a V_{OC} of 1.3 V, approaching the sum of the individual subcell voltages. An impressive fill factor of 70% is achieved, further confirming that the subcells are efficiently connected via an appropriate recombination layer.

*Corresponding authors.
E-mail addresses: pierre.beaujuge@kaust.edu.sa (P.M. Beaujuge), aram.amassian@kaust.edu.sa (A. Amassian).

http://dx.doi.org/10.1016/j.nanoen.2015.08.010
2211-2855/

Introduction

Solution-processed emerging thin film solar cells, such as devices based on organic and colloidal quantum dot (CQD) light absorbers, offer low-temperature processing, mechanical flexibility and conformability, lightweight modules, and compatibility with continuous roll-to-roll manufacturing [1-5]. Each of these is today limited to ca. 10% power conversion efficiency (PCE) in single-junction devices [6-9]. Multi-junction solar cell architectures that can harvest a broader portion of the solar spectrum are of interest to both the CQD and the organic solar cell communities [10-14]. Quantum dot solids benefit from a size-tunable bandgap that allows absorbing a relatively wide range of wavelengths from the visible to the near infrared [4,5,13,14]. Meanwhile, organic absorbers tend to have a narrower spectral absorption compared to quantum dot solids, making double (tandem) and triple-junction organic solar cells especially attractive, with published power conversion efficiency values of up to ca. 12% [15,16]. While CQD tandem solar cells have received limited attention thus far, a few CQD tandem cells have been reported with an ideal open circuit voltage (V_{OC}) equal to the sum of the two subcells (i.e. $\sim$1.0 V), yet those have not shown a convincing efficiency enhancement mainly due to their modest fill factors (FF) ($<$50%) [13,14]. On the other hand, a key advantage of polymer tandem solar cells is their ability to achieve both high V_{OC} (i.e. $>$1.5 V) and FF (i.e. $>$65%) [15,16]. Therefore, the opportunity exists to expand beyond the spectral range of organic absorbers and to compensate for the low FF of CQD cells by combining the two material types into a hybrid tandem solar cell which may eventually overcome the respective limitations of "all-CQD" and "all-polymer" multi-junction solar cells [17].

Here we report a hybrid tandem solar cell that combines solution-processed depleted-heterojunction CQD [18] and bulk heterojunction polymer:fullerene subcells [19,20]. The tandem is monolithically integrated and electrically connected in series with the aid of a suitable p-n recombination layer that includes metal oxides and a conjugated polyelectrolyte, and achieves high V_{OC} values and excellent FFs in the 60-70% range [21-24]. We discuss the monolithic integration of the subcells, taking into account solvent interactions with underlayers and associated constraints on the tandem architecture, and show that an adequate device configuration consists of a low bandgap CQD bottom cell and a high bandgap polymer:fullerene top cell. Once the recombination layer and individual subcells are optimized, the hybrid tandem device reaches a V_{OC} of 1.3 V, approaching the theoretical sum of the individual subcells. A FF of ca. 70% is achieved, which is higher than either of the CQD or polymer:fullerene single-junction cells, indicating that the subcells are efficiently connected via an appropriate recombination layer. Overall, the best hybrid tandem devices yield $>$5% PCE, demonstrating an efficient monolithic integration of CQD and polymer:fullerene subcells, and paving the path to achieving high-efficiency hybrid tandem solar cells via appropriate solution formulations, selected interlayers, and adequate vertically-stacked configurations.

Experimental section

Single-junction depleted-heterojunction colloidal QD solar cell fabrication

Pre-patterned fluorine-tin-oxide (FTO, 15 Ω/sq, Xin Yan LTD.) coated glass substrates were cleaned by sonication in Extran 300 detergent solution, deionized (DI) water, acetone and isopropanol in 20 min sequential steps. Next, the substrates were blown dry by N_2 and then coated with TiO_2 nanoparticles (Dyesol) by spin-coating the diluted TiO_2 solution in ethanol (1:3 by weight) at 1500 rpm, followed by heating at 80 °C for 5 min and 500 °C for 30 min on a hotplate. The substrates were cooled down to room temperature, and the $TiCl_4$ treatment was performed by immersing the substrates in a 120 mM solution in DI water at 70 °C for 30 min, then the substrates were rinsed with DI water and heated at 500 °C for 30 min. All the procedures for the TiO_2 coating step were carried out in ambient air conditions and the substrates were stored in the N_2 glovebox after TiO_2 coating.

The quantum dot film was formed through layer-by-layer deposition of PbS CQDs (50 mg/ml in octane). For each layer, two drops (50 μl) of CQDs were cast onto the substrates through a 0.2 μm filter and spin-coated at 2500 rpm for 10 s. Next, ca. 300 μl mercaptopropionic acid (MPA) in acetonitrile (ACN) solution (1% in volume) was used to fully cover the CQD surface and kept on the surface for 3 s, the solution was then removed by spining the sample at 2500 rpm for 5 s. Finally, the CQD surface was rinsed by casting and spinning ACN at 2500 rpm and this step was repeated twice: 5 s for the first rinse and 10 s for the second rinse. The QD deposition procedure was repeated 4 times. The PbS QD active layer has an extonic peak at 1.29 eV (960 nm) which corresponds to an average dot diameter of 3.1 nm, based on an empirical relationship between the first absorption peak position and dot size [25]. The QD-coated substrate was then transferred to a vacuum evaporator inside the N_2 glovebox. The evaporator chamber was evacuated to 2×10^{-6} Torr for the deposition of 16 nm MoO_x (Sigma Aldrich) at a rate of 0.3 Å/s, followed by 10 nm of gold (0.2 Å/s), and 80 nm of Ag (0.2 Å/s for the first 10 nm and 5 Å/s for the following 70 nm) as an electrode.

Single-junction inverted bulk heterojunction polymer:fullerene solar cell fabrication

Pre-patterned indium tin oxide (ITO, 15 Ω/sq, Xin Yan LTD.) coated glass substrates were cleaned by the same method as that used with FTO-coated glass. For the electron transporting layer (ETL) fabrication on cleaned ITO-coated glass, ZnO powder (Sigma Aldrich) was vacuum-evaporated using a tungsten boat at a deposition rate of 0.3 Å/s in a base pressure of 6×10^{-6} Torr, followed by a conjugated polyelectrolyte, poly[(9,9-bis(3′-(*N*,*N*-dimethylamino)propyl)-2,7-fluorene)-alt-2,7-(9,9-dioctylfluorene)] (PFN) (1-Materials) spin-coating at 5000 rpm for 60 s. The concentration of the PFN solution in ethanol was 1 mg/ml and a small amount of acetic acid (2 μl/ml) was added. The organic

photoactive layer was prepared by spin-coating at 900 rpm on ITO glass/ZnO/PFN either a blend solution of 10 mg of PBDTTT-C-T (1-Materials) and 18 mg of $PC_{71}BM$ (American Dye Sources) or 10 mg of PTB7 (1-Materials) and 15 mg of $PC_{71}BM$ in 1 ml of chlorobenzene (CB) with diiodooctane (DIO) 3 vol%. The substrates were then transferred to a thermal evaporator in a glovebox with N_2 atmosphere, and the evaporator chamber was evacuated to 2×10^{-6} Torr for electrode deposition. The device was completed with deposition of a 5 nm MoO_x layer (0.3 Å/s), followed by an 80 nm Ag layer (5 Å/s).

Solvent compatibility test with underlying photoactive materials

Solvent treatments simulating top-cell photoactive layer deposition were performed on the complementary photoactive layers. To test the compatibility of organic photoactive layer deposition with the underlying QD film, we spun CB containing 3 vol% DIO directly on top of the QD active layer at 900 rpm for 60 s. To test the compatibility of QD layer deposition, including ligand exchange and rinsing, with the underlying organic layer, we spun octane on the organic active film at 2500 rpm for 10 s, followed by ACN containing 1 vol% MPA casting for 3 s and spinning at 2500 rpm for 5 s, and rinsing with ACN by casting the latter and spinning at 2500 rpm for 5 s and repeating the same step for 10 s. This entire procedure was repeated up to 4 times, representing the full QD active layer formation. To proceed with device testing, the appropriate top electrodes were deposited after solvent treatment either on the organic or the QD photoactive layer.

Hybrid tandem solar cell fabrication

The structure of the hybrid tandem solar cell adopted in this study is a glass/FTO/TiO_2/QD/MoO_x/ZnO/PFN/polymer:fullerene/MoO_x/Ag. The fabrication procedure of the active layers is identical to the respective single-junction cells. The recombination layer consisted of MoO_x (0.3 Å/s) and ZnO (0.3 Å/s) deposited at a base pressure of 2×10^{-6} Torr in sequence by thermal evaporation, followed by spin-coating of the PFN layer at 5000 rpm for 60 s. The device fabrication was completed by thermal evaporation of MoO_x (5 nm) and Ag (80 nm) as the reflective top electrode. The active area of single-junction and tandem cells was 0.1 cm^2.

Electrical, optical, and microscopic characterization of solar cells and thin films

The *J-V* characteristics of the solar cells were measured using a Keithley 2400 source unit under AM 1.5 simulated illumination with an intensity of 100 mW/cm^2. A Xenon arc lamp (300 W) serves as the light source and the light intensity was calibrated using a KG5 filtered Si diode to reduce the spectral mismatch. Device parameters were averaged over 10 devices. The external quantum efficiency (EQE) measurements were performed at zero bias by illuminating the device with monochromatic light supplied from a Xenon arc lamp in combination with a dual-grating monochromator. Absorption spectra were taken using a Varian Cary 6000i ultraviolet-visible spectrophotometer with the integrating sphere. For Kelvin probe measurement (KP technology, SKP series), the relevant thin films (PFN, ZnO, MoO_x/ZnO and MoO_x/ZnO/PFN) were deposited on ITO-coated glass.

Optical modeling

Optical constants including real and imaginary refractive indexes (n, k) of PBDTTT-C-T:$PC_{71}BM$, PTB7:$PC_{71}BM$, TiO_2, MoO_x, ZnO, PFN, and Ag layers were measured by variable angle spectroscopic ellipsometry (VASE). The n value of QD film was measured by ellipsometery and the k values of the QD film was determined from UV-vis-NIR spectroscopy measurements using the formula, $k=\alpha\lambda/4\pi$ (α: absorption coefficient, λ: wavelength). The refractive index of FTO in the range of wavelengths from 380 nm to 1200 nm was provided by Xin Yan Technology LTD. from which FTO glass was purchased.

Results and discussion

In Fig. 1(a) we show the material systems used throughout this study: a PbS quantum dot with an organic 3-mercaptopropionic acid (MPA) ligand [26-28] for the bottom cell, as well as the chemical structures of the polymer donors [19,20] making up

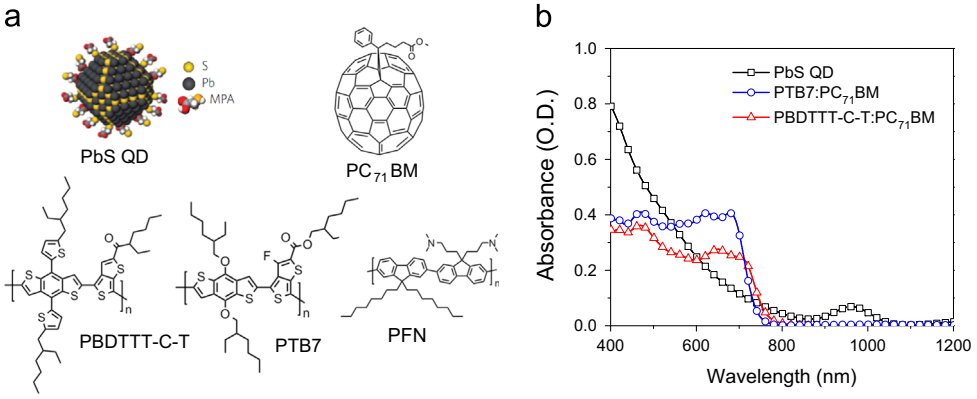

Fig. 1 (a) Materials chart, including a PbS quantum dot after ligand exchange, PBDTTT-C-T and PTB7 polymer donors, $PC_{71}BM$ as the fullerene acceptor and the conjugated polyelectrolyte PFN. (b) Absorption spectra of PbS CQD film and polymer: $PC_{71}BM$ active layers.

the top cell, and the polyelectrolyte used in the recombination layer. Two different polymer donors are studied, namely poly {[4,8-bis-(2-ethyl-hexyl-thiophene-5-yl)-benzo[1,2-*b*:4,5-*b*0] dithiophene-2,6-diyl]-alt-[2-(20-ethyl-hexanoyl)-thieno[3,4-*b*] thiophen-4,6-diyl]} (PBDTTT-C-T) and thieno[3,4-*b*]thiophene/ benzodithiophene (PTB7), in conjunction with the fullerene acceptor [6,6]-phenyl-C_{70}-butyric acid methyl ester ($PC_{71}BM$), forming the bulk heterojunction subcell. The conjugated polyelectrolyte PFN is used as part of the p-n recombination layer otherwise consisting of MoO_x and ZnO [20-23].

The depleted-heterojunction CQD solar cells were fabricated by constructing the QD active layer on TiO_2 in a sequential layer-by-layer (LbL) process that involved the repeated deposition of an oleic acid (OA)-capped QD layer, followed by a solid-state ligand-exchange and solvent wash between each step. The solid-state ligand-exchange of the OA molecules with MPA was performed from an acetonitrile (ACN) solution [26,27]. The thickness of the QD active layer after 4 LbL steps is ca. 140 nm (the thickness of each QD layer is ca. 40 nm, but due to the infiltration of the first QD layer into TiO_2 layer, the actual total thickness of the QD active layer is less than the sum of the layers), which corresponds to approximately 40% of the optimal active layer thickness in a single-junction CQD device. In Fig. 1(b) we show the absorption spectra of the active layers: a 140 nm QD film, a 120 nm PBDTTT-C-T:$PC_{71}BM$ and a 140 nm PTB7:$PC_{71}BM$ active layer. The QD active layer has a wide absorption spectrum covering the visible spectrum and extends into the near-infrared (NIR) 800-1050 nm [14], while the polymer: fullerene blends absorb effectively in the range 300-750 nm and transmit the NIR part of the spectrum.

One of the major challenges in the fabrication of solution-based tandem solar cells includes the selection of the proper recombination layer which must electrically connect the two subcells, while physically separating them [11-14]. It should be noted that, when the recombination layer is deposited via solution-processing techniques, improper solvents can damage the underlayers, and post-processing thermal annealing of the recombination layer can have undesirable effects on the underlayers as well [11,28]. Therefore, in this study, we chose to prepare the two metal oxide interlayers making up the recombination layer by vacuum deposition, all the while maintaining the substrate at room temperature. One of the most important solution-processing criteria of the top cell is the orthogonality of its solvent to the active layer of the bottom cell and to the recombination layer. Thus, the bottom cell may be damaged if the solvent(s) used to fabricate the top cell partially dissolve the active layer of the bottom cell, even in the presence of an effective recombination layer. Those issues can be amplified in the presence of pinholes or cracks in the recombination layer. In Fig. 2, we tested the orthogonality of the solvents (see the Experimental section) used in organic and QD subcell fabrications in order to probe the possibility of fabricating the QD subcell as a top cell using published formulations [28]. We first assess the

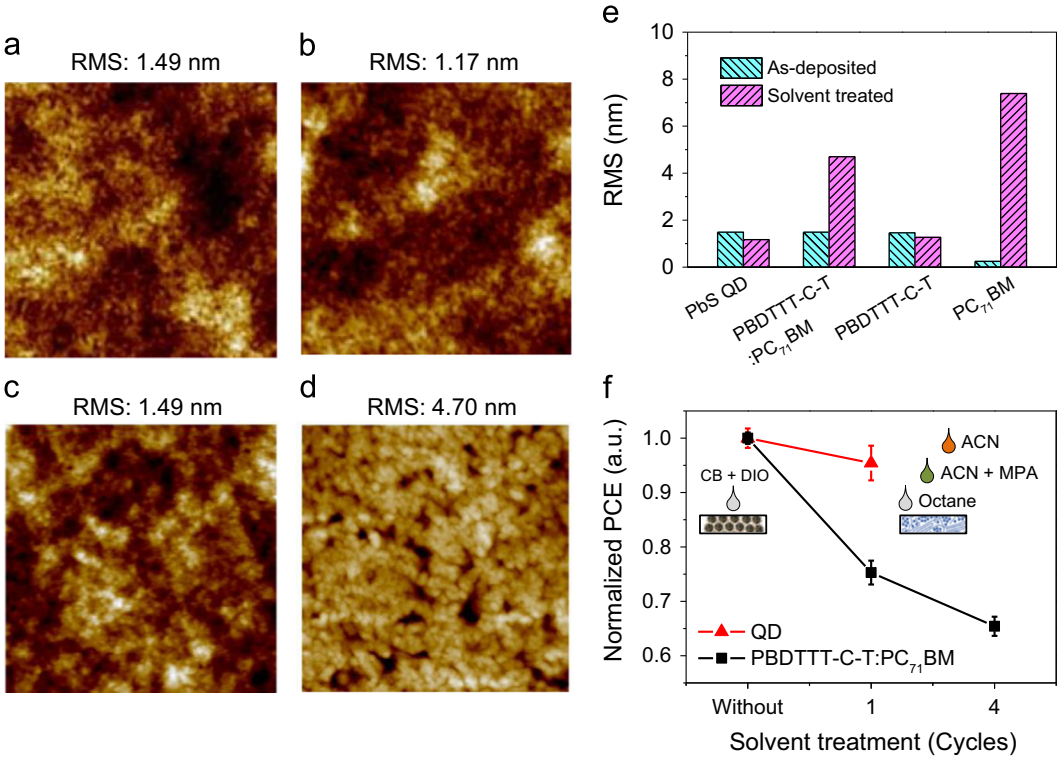

Fig. 2 (a) AFM images of surface topography for as-deposited PbS QD active layer subjected to ligand exchange and (b) after subsequent treatment with CB and 3 vol% DIO to simulate organic photoactive layer deposition. (c) AFM images of the surface topography of as-deposited PBDTTT-C-T:$PC_{71}BM$ active layer and (d) after subsequent treatment with octane to simulate QD photoactive layer deposition. The scan size is 1 μm × 1 μm. (e) Summary of RMS surface roughness of pristine and solvent-treated QD and organic thin films. (f) Normalized PCE of single-junction cells based on pristine and solvent-treated photoactive layers used in order to identify which underlayers can potentially withstand the process formulations of the overlayers.

orthogonality of the solvents by evaluating and comparing the surface morphology of the QD and the polymer:fullerene active layers before and after exposure to several solvents, and then fabricate and test the single junction solar cells after solvent exposure.

We test the effects of building the organic subcell on the QD cell by spin-coating chlorobenzene (CB) with 3 vol% DIO directly on the QD active layer at 900 rpm for 60 s. Vice versa, the effect of building the QD subcell on the polymer:fullerene cell is tested by spin-coating octane on the polymer active layer at 2500 rpm for 10 s. In Fig. 2(a) we show the atomic force microscopy (AFM) images of the surface morphology of an as-prepared PbS QD active layer on glass/FTO/TiO_2. Treating the QD film with CB and 3 vol% DIO impacts the morphology of the film negligibly, as shown in Fig. 2(b). In contrast, the polymer:fullerene blends appear to undergo significant morphological changes under the QD processing solvent conditions. In Fig. 2(c) and (d) we show the surface morphology of as-deposited and octane-treated PBDTTT-C-T:$PC_{71}BM$ bulk heterojunction blends cast on top of a PFN/ZnO/ITO/glass substrate, respectively. Here, the solvent treatment results in significant morphological roughening, which may be due to the rearrangement of the polymer and fullerene domains within the photoactive layer. In Fig. 2(e) we compare the root mean squared (RMS) surface roughnesses of the QD and polymer:fullerene active layers before and after treatment with the overlayer process solvents. The RMS roughness of the polymer:fullerene blend increased from 1.5 nm to 4.7 nm, indicating significant solvent-film interactions. Further investigations reveal that the octane selectively dissolves $PC_{71}BM$ (Figs. 2(e) and S1). In Fig. 2(f), the normalized PCE of the solvent-treated QD and PBDTTT-C-T:$PC_{71}BM$ single-junction cells is plotted as a function of the number of solvent treatment cycles to which the bottom subcell is subjected. As expected, a one-time exposure of the QD active layer to CB with 3 vol% DIO yields a negligible drop in PCE, whereas the polymer:fullerene single-junction cells are significantly affected by the exposure to common processing and ligand exchange solvents and chemicals [28], losing 25% of initial PCE after a single solvent treatment step and nearly 40% after four steps. From these experimental results, it can be concluded that the monolithic integration of the solution-processed subcells is more readily achievable by stacking the polymer:fullerene subcell on top of the QD bottom subcell. Additional considerations also favor this subcell configuration: efficient depleted-heterojunction QD solar cells require the use of inorganic electron transporting layers (TiO_2 or ZnO) which involve a high temperature annealing step (200–500 °C) to work effectively [18,24], and thermal annealing can severely damage the polymer:fullerene subcell if QD cell is stacked as a top subcell.

In Fig. 3(a) we illustrate the optimized hybrid tandem device configuration composed of a bottom QD subcell and a top polymer:fullerene cell. The cross-sectional transmission electron microscopy (TEM) image of a device using PBDTTT-C-T:$PC_{71}BM$ as active layer is also shown. The schematic energy diagram of the various layers involved in the hybrid tandem solar cell is shown in Fig. 3(b) [1,3,18–21]. The PbS QD active layer was deposited using the LbL process on a TiO_2 layer prepared on a FTO-coated glass substrate. The recombination layer consists of a vacuum-deposited layer of MoO_x used as hole transporting layer and a vacuum-deposited layer of ZnO passivated with a solution-coated PFN [21–23] acting concurrently as the electron transporting bilayer connected to the inverted polymer:fullerene top-cell. The conjugated polyelectrolyte is intended to passivate trap states present in the vacuum-evaporated ZnO layer, leading to improved solar cell characteristics [8,31–34]. The solution-processed polymer:fullerene bulk heterojunction layer was subsequently spin-cast and the tandem stack was completed by vacuum evaporation of MoO_x and Ag through a shadow mask. In Fig. S2, we show the work function values obtained by Kelvin probe measurements for ZnO and MoO_x/ZnO without and with the PFN layer, using ITO as a reference. The work functions of ZnO and MoO_x/ZnO were effectively decreased from −4.48 eV and −4.49 eV, respectively, to −3.84 eV and −3.95 eV, by applying the PFN treatment. This indicates that the PFN layer forms an interfacial dipole layer pointing away from the ZnO surface toward the polymer subcell, thus decreasing the effective ZnO work function [31–35]. The conduction band of ZnO (−4.4 eV) is slightly higher than the LUMO (−4.3 eV) of $PC_{71}BM$[1,10] as shown in Fig. 3(b). But with the insertion of the PFN layer, the work function value of ZnO is effectively decreased leading to an Ohmic contact with $PC_{71}BM$. This enhances the built-in potential and reduces the contact resistance between the polymer:fullerene bulk heterojunction layer and the recombination layer. Yang et al. [23,29–35] have also reported that PFN can reduce the charge trapping at the interface between polymer active layer and metal oxide as well [34].

In Fig. 3(c) we show the representative current density-voltage (*J*-*V*) characteristics obtained for the single-junction subcells. The device configuration of the QD cell is glass/FTO/TiO_2/PbS QDs/MoO_x/Au/Ag and yields a V_{OC} of 0.57 V, J_{SC} of 14.4 mA/cm^2, FF of 44.0%, resulting in a PCE of 3.6%. The configuration of the inverted polymer:fullerene single-junction cells is glass/ITO/ZnO/PFN/PBDTTT-C-T:$PC_{71}BM$ or PTB7:$PC_{71}BM$/MoO_x/Ag. The PBDTTT-C-T:$PC_{71}BM$ (PTB7:$PC_{71}BM$) single-junction cell yields a V_{OC} of 0.76 V (0.75 V), J_{SC} of 15.7 mA/cm^2 (16.1 mA/cm^2), and FF of 61.7% (64.2%), resulting in a PCE of 7.4% (7.7%). The V_{OC} of PBDTTT-C-T-based single-junction cells is slightly higher than that of the PTB7-based devices, but the J_{SC} and FF remain somewhat lower than those of the PTB7-based organic cells (Table 1). The external quantum efficiency (EQE) curves of the single-junction QD and organic cells are presented in Fig. 3(d). The QD cell harvests light up to ca. 1100 nm and also overlaps with the EQE spectra of the polymer cells at shorter wavelengths. PTB7-based cells exhibit slightly higher EQE in the range from 500 nm to 700 nm as compared to PBDTTT-C-T-based cells, explaining the slightly higher J_{SC} of single-junction cells using PTB7. The EQE of the QD cell is >50% in the range 300–600 nm and drops quickly after 600 nm, where the EQE of the polymer:fullerene cell is particularly pronounced (>60%; 600–750 nm).

The thickness of the recombination layer for the hybrid tandem solar cells was optimized by attempting several thickness combinations for the evaporated MoO_x/ZnO pair, namely 7.5 nm/10 nm, 7.5 nm/5 nm, 10 nm/5 nm and 12.5 nm/5 nm, followed by deposition of a PFN layer of constant thickness (ca. 3 nm). The initial optimization was performed using PBDTTT-C-T:$PC_{71}BM$ as the polymer:fullerene subcell. The optimized conditions were subsequently transferred to PTB7:$PC_{71}BM$, where the MoO_x/ZnO thickness

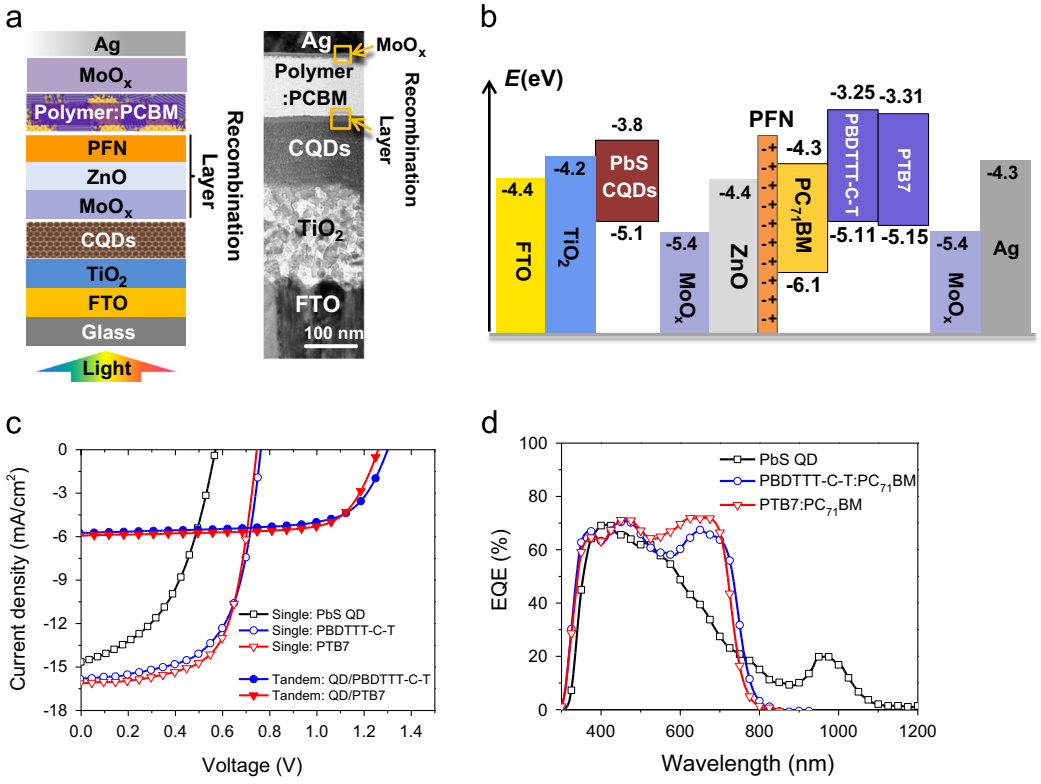

Fig. 3 (a) Hybrid tandem solar cell configuration and TEM cross-sectional image (polymer active layer: PBDTTT-C-T:$PC_{71}BM$) adopted for this study. (b) Energy level diagram for the hybrid tandem device. (c) Representative *J-V* characteristics of the single-junction and hybrid tandem cells (optimized recombination layer). (d) EQE spectra of the QD and polymer:fullerene single-junction cells.

Table 1 Average parameters of the QD and the polymer:fullerene single-junction cells.

Active layer	V_{OC} (V)	J_{SC} (mA/cm^2)	FF (%)	PCE (%)	Max. PCE (%)
PbS QD	0.573	14.44	44.01	3.64	3.87
PBDTTT-C-T:$PC_{71}BM$	0.758	15.74	61.67	7.36	7.43
PTB7:$PC_{71}BM$	0.745	16.07	64.22	7.69	7.82

was nevertheless varied (10 nm/5 nm vs 12.5 nm/5 nm) for comparison. In Fig. S3 we plot the *J-V* curves of polymer single-junction cells of PBDTTT-CT:$PC_{71}BM$ and tandem cells of PbS QD/PBDTTT-C-T:$PC_{71}BM$ with a recombination layer thickness of 10 nm/5 nm both without and with a PFN layer on top. All of the device figures of merit increased upon inclusion of PFN (Table S1), indicating that PFN effectively enhances the built-in potential and reduces the contact resistance between the organic photoactive layer and the interlayers [20-23,29,35].

In Fig. 4 we show the statistical distribution of the figures of merit for hybrid tandem devices made with PBDTTT-C-T:$PC_{71}BM$ and PTB7:$PC_{71}BM$. The representative *J-V* plots are shown in Fig. S4(a) and (b), respectively. One of the best tandem device performance was obtained for PbS QD/PBDTTT-C-T:$PC_{71}BM$ with a recombination layer made of 10 nm MoO_x and 5 nm ZnO, yielding a high V_{OC} of 1.3 V and a FF of 68.1%. In comparison, the recombination layer made of 12.5 nm/5 nm MoO_x/ZnO performed more modestly, resulting in lower FF values (see Table 2) and confirming the importance of optimizing the configuration of the recombination layer in hybrid tandem devices. The hybrid tandem based on PbS QD/PTB7:$PC_{71}BM$ with the same recombination layer as the best PbS QD/PBDTTT-C-T:$PC_{71}BM$ tandem yielded a V_{OC} of 1.25 V and a FF of 69.2%. The PCE of hybrid tandems made with PTB7:$PC_{71}BM$ is slightly higher than tandems based on PBDTTT-C-T:$PC_{71}BM$, mainly due to higher FF and J_{SC}. Importantly, the characteristics of the tandem devices for the respective polymer donors are well aligned with the performance of the respective single-junction cells, achieving slightly higher PCE values with PTB7 compared to PBDTTT-C-T (Fig. 3(c)).

The V_{OC} of the hybrid tandem device made with the optimized recombination layer configuration reached 1.3 V in the case of PBDTTT-C-T:$PC_{71}BM$, representing 97% of the sum of the V_{OC} values of the individual cells. The FF of the hybrid tandem devices based on PTB7 improved significantly compared to those of the individual single-junction cells, reaching ~70% in the best condition of hybrid tandem device. The high FF is attributed to efficient recombination

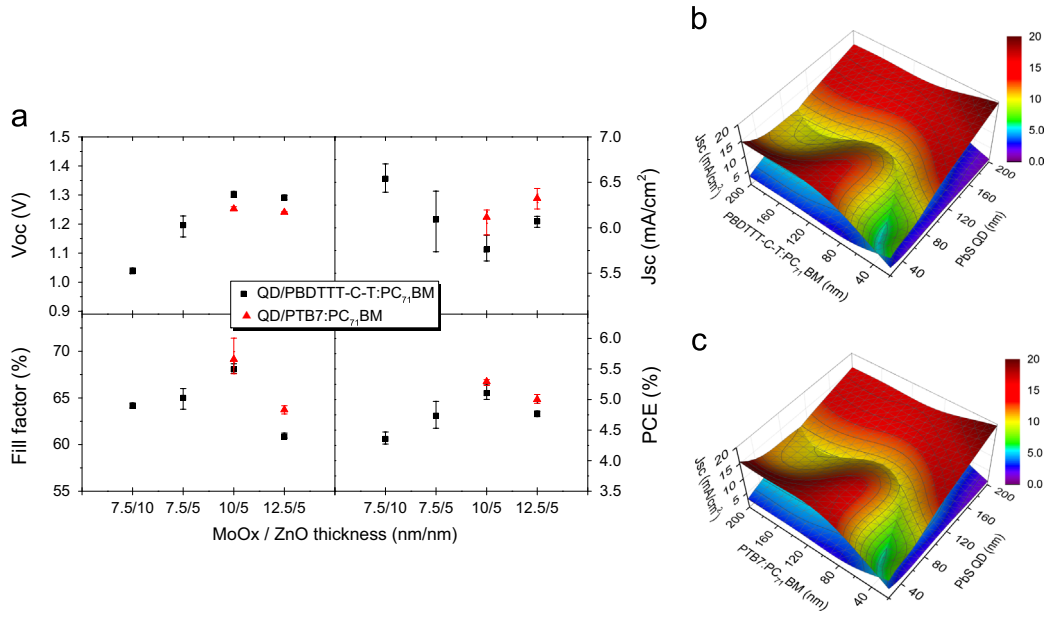

Fig. 4 (a) Statistical summary of the hybrid tandem solar cell parameters as a function of the recombination layer thickness of MoO_x/ZnO (Error bars show the minimum and maximum values). A PFN layer was cast on ZnO in all cases. (b) Simulated J_{SC} of the hybrid tandem solar cells as a function of active layer thickness: PBDTTT-C-T:$PC_{71}BM$ and PbS QD, (c) PTB7:$PC_{71}BM$ and PbS QD, the cross-matched interface of the surface plot shows the current matched values, the contour is drawn by 1 mA/cm^2.

Table 2 Average parameters of hybrid tandem solar cells depending on the thickness of MoO_x and ZnO in the MoO_x/ZnO/PFN recombination layer and on the choice of the polymer donor.

Polymer active layer (donor: $PC_{71}BM$)	MoO_x (nm)	ZnO (nm)	V_{OC} (V)	J_{SC} (mA/cm^2)	FF (%)	PCE (%)	Max. PCE (%)
PBDTTT-C-T	7.5	10	1.038	6.54	64.15	4.35	4.47
PBDTTT-C-T	7.5	5	1.196	6.09	65.00	4.73	4.97
PBDTTT-C-T	10	5	1.302	5.76	68.09	5.11	5.25
PTB7	10	5	1.252	6.12	69.15	5.29	5.33
PBDTTT-C-T	12.5	5	1.291	6.07	60.85	4.77	4.81
PTB7	12.5	5	1.241	6.32	63.74	5.00	5.08

of the electron and hole at the ZnO/MoO_x interface, which reduces the contact resistance and the space charge build up within the active layers [36-38]. Overall, the high V_{OC} and FF values reached indicate that the two subcells are effectively connected in series.

Additionally, to know whether the high FF of our hybrid tandem cell is a result of light filtering effect by the subcells, we investigated the relation between FF change and light filtering effect for each subcell. First, we fabricated a semitransparent QD single-junction cell consisting of the following transparent top electrode: MoO_x 20 nm/Au 1 nm/Ag 6.5 nm/MoO_x 20 nm/LiF 60 nm [39], which had a sheet resistance of 19.5 Ω/sq (Fig. S5). To test the FF change of the QD subcell caused by the decrease of the reflected light due to the light absorption of the polymer active layer as a top subcell, we inserted a polymer light filter between the mirror and the semitransparent (single pass) QD cell as shown in Fig. S6(a) and (b). The polymer light filter consisted of a PTB7:$PC_{71}BM$ active layer coated on glass. A second light pass was made possible using a Ag-coated (150 nm) glass mirror. The change in FF of the QD single-junction cell with and without the polymer filter was found to be less than 1% (Table S2), meaning that the light intensity reduction due to subcell filtering does not contribute to the FF enhancement in the hybrid tandem device. The trend in FF for the QD cell is similar to that described in earlier work [40], where the FF of PbS QD solar cells was found to be nearly constant irrespective of incident light intensity. The PTB7:$PC_{71}BM$ single-junction solar cell showed a FF increase of only ~2% when using the QD subcell as a light filter (Fig. S6(c) and (d)). The filtering of the incident light intensity improved the FF of the polymer BHJ cell only slightly (which is a general characteristic of polymer solar cells [41]). Our analysis therefore indicates that light filtering by adjacent subcells does not contribute significantly to the substantial FF improvement shown in the hybrid tandem cell, in which a maximum FF as high as ca. 70% was achieved vs. 64% (44%) in the polymer (CQD) single-junction cells, pointing instead to the quality of electrical interconnection of the subcells via an appropriate recombination layer.

The highest PCE obtained for the hybrid tandem cells made with PTB7 is ca. 5.3%, which represents a significant improvement over the QD single-junction cell alone. The tandem efficiency remains however lower than the peak efficiency of the best PTB7:$PC_{71}BM$ single-junction cells because of the J_{SC}

limitations in the tandem device. We simulated the optimum thickness of each subcell's active layer for the maximum current matching in these hybrid tandem solar cells using the Setfos, simulation software (Fluxim AG, Switzerland). The optical parameters (n, k) of the various materials and their thicknesses were used as input parameters [42] for the optical modeling (summarized in Fig. S7). Fig. 4(b) and (c) shows the surface plots of the calculated J_{SC} as a function of the active layer thickness of each subcell. The maximum J_{SC} of the hybrid tandem solar cell corresponds to the cross-matched value of the two subcell surface plots, from which the optimum thicknesses of PBDTTT-C-T:$PC_{71}BM$ and PbS QD active layers can be expected to be ca. 110 nm and 113 nm with J_{SC} of 10.2 mA/cm^2, and those of PTB7:$PC_{71}BM$ and PbS QD to be ca. 110 nm and 118 nm with J_{SC} of 10.5 mA/cm^2, respectively. The simulations agree with the experimental observation that PTB7-based tandem (Fig. 4(b)) produce slightly higher maximum J_{SC} than PBDTTT-C-T (Fig. 4(c)). In parallel, and on the basis of our optical modeling simulations, it is worth noting that the J_{SC} of the hybrid tandem solar cells may be expected to improve upon further reducing the thicknesses of the two subcells (actual subcell thicknesses discussed throughout this study: PBDTTT-C-T:$PC_{71}BM$, 120 nm; PTB7:$PC_{71}BM$, 140 nm; PbS QD, 140 nm).

The lack of spectral complementarity between the QD and the polymer:fullerene subcells (Fig. 1(a)) is an important factor explaining the comparatively low J_{SC} in the hybrid tandem devices. Since visible light is first absorbed by the low-bandgap QD bottom cell, less visible light reaches the high-bandgap polymer:fullerene top cell, resulting in reduced exciton and free carrier generation in the top cell. In order to obtain higher J_{SC} values with the present hybrid tandem device configuration, alternative polymer donors with lower bandgaps (<1.6 eV) could help reinforce the NIR absorption of the hybrid tandem, while taking full advantage of the QD bottom cell visible absorption [12,30]. Another important approach will be to swap the QD and the polymer:fullerene subcells in the vertically-stacked tandem, which should significantly improve the visible absorption of the polymer:fullerene subcell as a bottom cell and its photocurrent. The QD subcell as a top cell may then be made thicker so as to harvest more light in the NIR region, thus maintaining a high photocurrent. It is worth noting, however, that swapping the subcells will require addressing the solvent formulation issues and developing a modified solid-state ligand exchange procedure that would prevent or considerably reduce the damage caused to the underlying recombination and photoactive layers.

Conclusions

In conclusion, we showed that QD and polymer:fullerene hybrid tandem solar cells can now achieve $>5\%$ PCE upon optimization of the recombination layer (MoO_x/ZnO) with an effective conjugated polyelectrolyte layer. The hybrid tandem devices show V_{OC} values of up to 1.3 V that correspond to the sum of the V_{OC} of the individual subcells, and high FFs of ca. 70% that surpass the FFs of the individual subcells. The systematic optimization of the recombination layer led to an effective connection of the QD and polymer:fullerene subcells in series, resulting in a two-terminal device of particularly high FF values. Combined with a careful optimization of individual subcell, the champion hybrid tandems are more efficient than the QD single-junction cells alone. Overall, the QD and polymer:fullerene hybrid tandem approach paves the path to (i) extending the spectral absorption of polymer:fullerene single-cell and tandem devices via the integration of the QD subcell, and (ii) notably improving the performance of QD single-cell and tandem devices by absorbing visible light more effectively and by widening the device V_{OC}. The next steps towards monolithic integration will require further developments in the area of process formulations so as to achieve the necessary underlayer compatibility, and the optimum device configuration. Following this approach, two or more solution-processed subcells composed of complementary organic and inorganic light absorbers illuminated in an adequate sequence should be achievable.

Acknowledgements

This publication is based in part on work supported by Award KUS-11-009-21, made by King Abdullah University of Science and Technology (KAUST), by the Ontario Research Fund Research Excellence Program, and by the Natural Sciences and Engineering Research Council (NSERC) of Canada. Part of this work was supported by the KAUST Office of Competitive Research Funds under round 2 of the Competitive Research Grant. AA is grateful to SABIC for the Career Development SABIC Chair.

Appendix A. Supporting information

Supplementary data associated with this article can be found in the online version at http://dx.doi.org/10.1016/j.nanoen.2015.08.010.

References

[1] A.J. Heeger, Adv. Mater. 26 (2014) 10–28.
[2] P.M. Beaujuge, J.M. Fréchet, J. Am. Chem. Soc. 133 (2011) 20009–20029.
[3] J.Y. Kim, O. Voznyy, D. Zhitomirsky, E.H. Sargent, Adv. Mater. 25 (2013) 4986–5010.
[4] B.I. MacDonald, A. Martucci, S. Rubanov, S.E. Watkins, P. Mulvaney, J.J. Jasieniak, ACS Nano 6 (2012) 5995–6004.
[5] R.W. Crisp, M.G. Panthani, W.L. Rance, J.N. Duenow, P.A. Parilla, R. Callahan, M.S. Dabney, J.J. Berry, D.V. Talapin, J.M. Luther, ACS Nano 8 (2014) 9063–9072.
[6] C.-H.M. Chuang, P.R. Brown, V. Bulović, M.G. Bawendi, Nat. Mater. 13 (2014) 796–801.
[7] L. Huo, T. Liu, X. Sun, Y. Cai, A.J. Heeger, Y. Sun, Adv. Mater. 27 (2015) 2938–2944.
[8] L.K. Jagadamma, M. Al-Senani, A.E. Labban, I. Gereige, G.O. N. Ndjawa, J.C.D. Faria, T. Kim, K. Zhao, F. Cruciani, D. H. Anjum, M.A. Mclachlan, P.M. Beaujuge, A. Amassian, Adv. Energy Mater. 5 (2015) 1500204.
[9] ⟨http://www.nrel.gov/ncpv/images/efficiency_chart.jpg⟩.
[10] J.Y. Kim, K. Lee, N.E. Coates, D. Moses, T.-Q. Nguyen, M. Dante, A.J. Heeger, Science 317 (2007) 222–225.
[11] A. Hadipour, B. de Boer, P.W. Blom, Adv. Funct. Mater. 18 (2008) 169–181.
[12] L. Dou, J. You, J. Yang, C.-C. Chen, Y. He, S. Murase, T. Moriarty, K. Emery, G. Li, Y. Yang, Nat. Photonics 6 (2012) 180–185.

[13] X. Wang, G.I. Koleilat, J. Tang, H. Liu, I.J. Kramer, R. Debnath, L. Brzozowski, D.A.R. Barkhouse, L. Levina, S. Hoogland, E. H. Sargent, Nat. Photonics 5 (2011) 480–484.
[14] J.J. Choi, W.N. Wenger, R.S. Hoffman, Y.-F. Lim, J. Luria, J. Jasieniak, J.A. Marohn, T. Hanrath, Adv. Mater. 23 (2011) 3144–3148.
[15] W. Li, A. Furlan, K.H. Hendriks, M.M. Wienk, R.A.J. Janssen, J. Am. Chem. Soc. 135 (2013) 5529–5532.
[16] C.-C. Chen, W.-H. Chang, K. Yoshimura, K. Ohya, J. You, J. Gao, Z. Hong, Y. Yang, Adv. Mater. 26 (2014) 5670–5677.
[17] M.J. Speirs, B.G.H.M. Groeneveld, L. Protesescu, C. Piliego, M. V. Kovalenko, M.A. Loi, Phys. Chem. Chem. Phys. 16 (2014) 7672–7676.
[18] A.G. Pattantyus-Abraham, I.J. Kramer, A.R. Barkhouse, X. Wang, G. Konstantatos, R. Debnath, L. Levina, I. Raabe, M.K. Nazeeruddin, M. Gratzel, E.H. Sargent, ACS Nano 4 (2010) 3374–3380.
[19] L. Huo, S. Zhang, X. Guo, F. Xu, Y. Li, J. Hou, Angew. Chem. 50 (2011) 9697–9702.
[20] L. Lu, L. Yu, Adv. Mater. 26 (2014) 4413–4430.
[21] Z. He, C. Zhong, S. Su, M. Xu, H. Wu, Y. Cao, Nat. Photonics 6 (2012) 591–595.
[22] R. Xia, D.-S. Leem, T. Kirchartz, S. Spencer, C. Murphy, Z. He, H. Wu, S. Su, Y. Cao, J.S. Kim, J.C. deMello, D.D.C. Bradley, J. Nelson, Adv. Energy Mater. 3 (2013) 718–723.
[23] C.-C. Chen, L. Dou, J. Gao, W.-H. Chang, G. Li, Y. Yang, Energy Environ. Sci. 6 (2013) 2714–2720.
[24] H.-Y. Park, I. Ryu, J. Kim, S. Jeong, S. Yim, S.-Y. Jang, J. Mater. Chem. C 118 (2014) 17374–17382.
[25] I. Moreels, K. Lambert, D. Smeets, D. De Muynck, T. Nollet, J. C. Martins, F. Vanhaecke, A. Vantomme, C. Delerue, G. Allan, Z. Hens, ACS Nano 3 (2009) 3023–3030.
[26] A.H. Ip, S.M. Thon, S. Hoogland, O. Voznyy, D. Zhitomirsky, R. Debnath, L. Levina, L.R. Rollny, G.H. Carey, A. Fischer, K. W. Kemp, I.J. Kramer, Z. Ning, A.J. Labelle, K.W. Chou, A. Amassian, E.H. Sargent, Nat. Nanotechnol. 7 (2012) 577–582.
[27] G.H. Carey, K.W. Chou, B. Yan, A.R. Kirmani, A. Amassian, E. H. Sargent, MRS Commun. 3 (2013) 83–90.
[28] A.R. Kirmani, G.H. Carey, M. Abdelsamie, B. Yan, D. Cha, L. R. Rollny, X. Cui, E.H. Sargent, A. Amassian, Adv. Mater. 26 (2014) 4717–4723.
[29] Z. He, H. Wu, Y. Cao, Adv. Mater. 26 (2014) 1006–1024.
[30] Y.-M. Chang, C.-Y. Leu, J. Mater. Chem. A 1 (2013) 6446–6451.
[31] S. Woo, W.H. Kim, H. Kim, Y. Yi, H.-K. Lyu, Y. Kim, Adv. Energy Mater. 4 (2014) 1301692.
[32] J.W. Shim, C. Fuentes-Hernandez, Y. Zhou, A. Dindar, T. M. Khan, A.J. Giordano, H. Cheun, M. Yun, S.R. Marder, B. Kippelen, Adv. Energy Mater. 4 (2014) 1400048.
[33] J. Jo, J.-R. Pouliot, D. Wynands, S.D. Collins, J.Y. Kim, T. L. Nguyen, H.Y. Woo, Y. Sun, M. Leclerc, A.J. Heeger, Adv. Mater. 25 (2013) 4783–4788.
[34] H. Ma, H.-L. Yip, F. Huang, A.K.-Y. Jen, Adv. Funct. Mater. 20 (2010) 1371–1388.
[35] T.-S. Kim, S.-I. Na, S.-H. Oh, R. Kang, B.-K. Yu, J.-S. Yeo, J. Lee, D.-Y. Kim, Sol. Energy Mater. Sol. Cells 98 (2012) 168–171.
[36] A.R. bin Mohd Yusoff, S.J. Lee, H.P. Kim, F.K. Shneider, W.J. da Silva, J. Jang, Adv. Funct. Mater. 24 (2014) 2240–2247.
[37] M. Riede, C. Uhrich, J. Widmer, R. Timmreck, D. Wynands, G. Schwartz, W.-M. Gnehr, D. Hildebrandt, A. Weiss, J. Hwang, S. Sundarraj, P. Erk, M. Pfeiffer, K. Leo, Adv. Funct. Mater. 21 (2011) 3019–3028.
[38] J. Lee, H. Kang, J. Kong, K. Lee, Adv. Energy Mater. 4 (2014) 1301226.
[39] S. Schubert, J. Meiss, L. Müller-Meskamp, K. Leo, Adv. Energy Mater. 3 (2013) 438–443.
[40] J. Tang, K.W. Kemp, S. Hoogland, K.S. Jeong, H. Liu, L. Levina, M. Furukawa, X. Wang, R. Debnath, D. Cha, K.W. Chou, A. Fischer, A. Amassian, J.B. Asbury, E.H. Sargent, Nat. Mater. 10 (2011) 765–771.
[41] S.R. Cowan, A. Roy, A.J. Heeger, Phys. Rev. B 82 (2010) 245207.
[42] G.-H. Kim, B. Walker, H.B. Kim, J.Y. Kim, E.H. Sargent, J. Park, J.Y. Kim, Adv. Mater. 26 (2014) 3321–3327.

Taesoo Kim received his Ph.D. degree in Materials Science Engineering from Gwangju Institute of Science and Technology (GIST), Gwangju, Republic of Korea, in August 2012. He is currently working as a postdoctoral fellow in the Amassian group at Solar and Photovoltaics Engineering Research Center (SPERC) of the King Abdullah University of Science and Technology (KAUST), Saudi Arabia. His current research interests include the hybrid tandem solar cells using quantum dot, perovskite and polymer materials and optoelectronic devices.

Yangqin Gao received the M.S. degree from King Abdullah University of Science and Technology (KAUST), Thuwal, Saudi Arabia, in 2010. He is currently a Ph.D. student in Materials Science and Engineering working with Dr. Pierre M. Beaujuge at KAUST. His research interests include application of nanostructured materials for dust control in solar cell, and multi-junction polymer solar cell with polymeric absorbers and hybrid absorbers.

Hanlin Hu received the M.S. degree from Tianjin University of Science and Technology, Tianjin, China, in 2012. He is currently a Ph.D. student in Materials Science and Engineering working with Dr. Aram Amassian at King Abdullah University of Science and Technology (KAUST). His research interests include organic semiconductor structure–property relationships and organic solar cells.

Buyi Yan received his bachelor degree from Zhejiang University and University of New South Wales. He is currently a Ph.D. student in Electrical Engineering, working with Dr. Aram Amassian at the King Abdullah University of Science and Technology (KAUST). His research interests include colloidal quantum dot solar cells.

Zhijun Ning received his Ph.D. degree at East China University of Science and Technology, under supervision of Prof. He Tian. From 2009 to 2011 he worked as a postdoctoral scholar at Royal Institute of Technology, Sweden. From 2011 to 2014, he was a postdoctoral scholar at University of Toronto, under supervision of Prof. Edward H. Sargent. At December 2014, he joined ShanghaiTech University as a faculty member. He is recipient of Young 1000 Talent Program. His research interest mainly focus on the synthesis and application of novel optoelectronic materials such as nanocrystals, perovskite, and organic molecules for solar cells, displays, photodetectors, and photocatalysis.

Lethy Krishnan Jagadamma is currently a postdoctoral fellow in the Amassian group in the Solar and Photovoltaics Engineering Research Center (SPERC) at the King Abdullah University of Science and Technology (KAUST), Saudi Arabia. Her research interests are mainly solution processed and vacuum evaporated metal oxides for optoelectronic devices such as organic and perovskite solar cells as well as light emitting diodes.

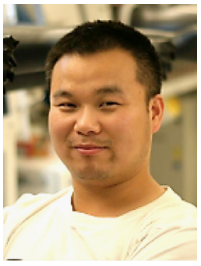

Kui Zhao received his Ph.D. degree in Materials Science Engineering from Chinese Academy of Science (CAS), China, in Jan 2010. He is currently working as a postdoctoral fellow in the Amassian group at the King Abdullah University of Science and Technology (KAUST), Saudi Arabia. His current research interests focus on renewable energy including perovskite solar cell, organic photovoltaics, quantum dots solar cell and organic electronics.

Ahmad R. Kirmani is currently a Ph.D. student working with Dr. Aram Amassian at the King Abdullah University of Science and Technology (KAUST), Saudi Arabia. He works in the area of colloidal quantum dot photovoltaics with special emphasis on surface characterization of nanomaterials using photoelectron spectroscopy.

Jessica Eid received her Ph.D. degree in Materials Science Engineering from Institut National Polytechnique de Grenoble (INPG), France in October 2007. She is currently working as a Research Scientist at Solar and Photovoltaics Engineering Research Center (SPERC) of King Abdullah University of Science and Technology (KAUST), Saudi Arabia. Her current research interests include the inorganic and hybrid materials for solar cells applications.

Michael Adachi is currently a postdoctoral fellow working with Prof. Sargent at the University of Toronto. He obtained his Ph.D. in 2012 and Master degree in 2007 in Electrical Engineering from the University of Waterloo and Simon Fraser University, respectively. His research interests include lasers and solar cells based on nanomaterials.

Ted Sargent holds the rank of University Professor at the University of Toronto. He is Canada Research Chair in Nanotechnology and serves as Vice Dean for Research for the Faculty of Applied Science and Engineering. He is a Fellow of the Royal Society of Canada (FRSC), FAAAS, and FIEEE for his contributions to the development of solar cells and light sensors based on solution processed semiconductors. He is the founder and CTO of InVisage Technologies and of Xagenic Inc.

Pierre M. Beaujuge is Faculty in the Materials Sciences & Engineering and in the Chemical Sciences Programs at King Abdullah University of Science & Technology (KAUST). He is also member of the Solar & Photovoltaics Engineering Research Center (SPERC) at KAUST. He received his Ph.D. from University of Florida in 2009, and worked as a Post-Doctoral Associate at University of California, Berkeley (2009–2010) and in the Materials Sciences Division of Lawrence Berkeley National Laboratory (2010–2011).

Aram Amassian holds the SABIC Chair and the rank of Associate Professor of Materials Science and Engineering at the King Abdullah University of Science and Technology (KAUST). He is a founding member of the KAUST faculty as well as a member of the Solar and Photovoltaic Engineering Research Center (SPERC) at KAUST. He received his Ph.D. in Engineering Physics from Ecole Polytechnique de Montreal (Canada), and worked as a NSERC postdoctoral fellow in the Malliaras group in Materials Science and Engineering at Cornell University (USA). The research in the Amassian group focuses on the science and engineering of solution-processed organic and inorganic semiconductors for electronic and emerging photovoltaic applications.